Two-Dimensional Lattice–Boltzmann Model of Hydrosol Depth Filtration

Hervé Duval, David Masson, and Jean-Bernard Guillot
Laboratoire de Génie des Procédés et Matériaux, École Centrale Paris, Grande Voie des Vignes, 92295 Châtenay-Malabry, France

Philippe Schmitz
Institut de Mécanique des Fluides de Toulouse, Allée du Professeur C. Soula, UMR CNRS 5502, 31400 Toulouse, France

Dominique d'Humières
Laboratoire de Physique Statistique, École Normale Supérieure, 24 Rue Lhomond, 75231 Paris Cedex 05, France

DOI 10.1002/aic.10606
Published online September 1, 2005 in Wiley InterScience (www.interscience.wiley.com).

A two-dimensional mathematical model of the initial stage of depth filtration is developed. This model describes the fluid flow and the particle transport and capture in a representative elementary volume of the filter. A typical simulation can be outlined as follows: as a first stage, the flow field is computed in the whole complex void space of the filter using a lattice–Boltzmann method. As a second stage, the trajectory analysis is derived by applying Newton's second law to suspended particles in the flowing fluid. The capture or the reentrainment of the particles encountering the filter surface is determined from a force balance that takes into account the drag force and the solid friction force. This approach, which provides both microscopic data such as the initial capture probability density and macroscopic data such as the filter coefficient, is validated on a model experiment of deep-bed filtration. © 2005 American Institute of Chemical Engineers *AIChE J,* 52: 39–48, 2006
Keywords: filtration, non-Brownian particles, porous media, hydrodynamics, lattice–Boltzmann model (LBM)

Introduction

Deep-bed filtration is a fluid–solid separation process commonly applied to remove minute quantities of small particles from various kinds of fluids. This engineering practice has a long history—Egyptian inscriptions show that deep-bed filtration was used for water treatment as early as 200 BC. Now this process has widespread applications from wastewater treatment to liquid metal refining and gas cleaning.

The basic principle of deep-bed filtration is the following (see Tien's book[1] for a comprehensive review): first, contrary to other kinds of filtration, the solid particles suspended in the fluid are typically smaller than the pores of the filtering medium. As the fluid–solid suspension flows through the filter, the particles present in the suspension deposit at various depths within the bed, that is, on the solid walls bordering the pore spaces. This leads to the progressive clogging of the filter and the subsequent increase of the pressure drop across it.

Thus, it is usual to divide the filtration process into two stages: initial and ageing stages. In the initial stage, the deposition of particles inside the filter is relatively small. Its effect on the properties of the filter is negligible, and the performance of the filter can be regarded as that of the clean filter. On the

Present address of P. Schmitz: INSA-GBA-LBB, Complexe Scientifique de Rangueil, 31077 Toulouse, Cedex 4, France.
Correspondence concerning this article should be addressed to H. Duval at herve.duval@ecp.fr.

contrary, the ageing stage corresponds to the clogging of the filter. In this report, we focus on the initial stage of depth filtration.

Numerous models have been proposed to simulate deep-bed filtration. They can be classified as follows: macroscopic, microscopic, stochastic, and networks.

The macroscopic model[1,2] is formulated for the purpose of describing the overall behavior of deep-bed filtration. In particular, it can predict the histories of the effluent concentration and the pressure drop across the filter. The model consists of the conservation equation of the particles, the assumed filtration rate expression, and the mechanics of the flow through the porous medium. Usually, the filtration rate is given by Iwasaki's phenomenological expression,[3] where the key parameter is the so-called filter coefficient. The average flow within the filter (as opposed to the local flow in the pore) is often considered one-dimensional and the macroscopic average velocity profile is considered flat. In the laminar regime, the pressure drop across the filter is typically modeled by the Darcy law combined with the Carman–Kozeny equation for the permeability. More recently, two-dimensional simulations have been performed solving the full set of macroscopic equations.[4] Thus, the macroscopic flow pattern through the filter has been obtained for different industrial configurations.

Whereas the macroscopic approach rather considers the filter as a "black box," the microscopic approach (also called trajectory analysis model) tries to explain the physics of the deposition processes within the filter. In this way, the microscopic approach attempts to quantitatively predict the filter efficiency. The filter is modeled as an assembly of individual collectors of some simple geometry (such as a capillary, a sphere, or a constricted tube). First of all, the flow field associated with the individual collector is obtained either analytically[1,5] or numerically.[6] Then, particle trajectories (around or through an individual collector) are calculated from the force balance that acts on the particle. The individual collector efficiency corresponds to the fraction of particles encountering the collector. Finally, the overall filter efficiency is deduced from the individual collector efficiency by simple association laws. The microscopic approach is well suited for evaluating the performance of the clean filter but it fails to predict permeability change during the filtration process.

The stochastic approach[7] models the pressure-head increase of a clogged filter. The pressure drop increase is viewed as resulting from two simultaneous stochastic processes, the blockage (arising from the accumulation of deposits within the pores) and the scouring of pores (arising from reentrainment of the deposits). The development of this birth–death process is governed by probabilistic laws whose parameters are adjusted to fit appropriate experimental data. Therefore, the stochastic model is a kind of "black box" as well and does not provide a precise description of the deposition mechanism.

In the network approach,[8-12] the porous medium is approximated by a network of tubes with a range of sizes distributed randomly in a two-dimensional square lattice; thus, the pore size distribution and the pore interconnectivity are taken into account. The fluid flow in such a network can be computed using a matrix expression for Darcy's law derived from electrical network theory. The formation of deposit during deep-bed filtration is taken into account by appropriately varying the diameter, and thus the flow resistance, of each tube. This model is essentially adapted to simulate the progressive clogging of the filter and its effects on flow pattern.

The model presented herein belongs to the microscopic approach. Whereas the standard microscopic approach focuses on a single collector, the present model describes fluid flow and particle transport and capture in a representative elementary volume of the filter, which consists of several interconnected pores. The flow field is computed in the whole complex void space of the representative elementary volume using a lattice–Boltzmann method (a comprehensive review can be found in Rothman and Zaleski[13]). This method is particularly suitable for investigating fluid flow at low values of the Reynolds number in complex geometry.

We limit the scope of our investigation to hydrosols. The suspended particles are non-Brownian, which means that the size of the focused particles is typically >1 μm. Furthermore, the interactions between the particles and the surface are supposed to be nonrepulsive. We assume that adhesive-surface forces provide negligible contribution to particle transport: this typically concerns particles > 10 μm. Finally, the lubrication effect on particle transport and capture is neglected. Indeed, the lubrication effect is assumed to be weak for irregularly shaped particles or rough filter walls (bordering the pores spaces). First elements confirming this assumption will be developed in this paper (see the passage relative to the *suspended particles* in the modeling section). A full study of the effect of particle shape and filter roughness on hydrodynamic interactions is left for future work.

The method is applied to a model experiment of deep-bed filtration developed by Frey et al.[14] First, microscopic (that is, at pore scale) results are interpreted and compared to the experimental observations of Frey et al.[14] Second, the method is used to calculate the initial filter coefficient, which is essential for the design and the global modeling of the deep-filtration process. The dependency of the initial filter coefficient on the filter grain size is predicted and its scaling behavior is compared to FitzPatrick's experimental data.[1]

Experiments of Frey et al.

Description

Frey et al.[14] performed pressure-driven deep-bed filtration experiments in a transparent etched micromodel (for a detailed description of the experiments, see Frey et al.[14] and Gohr Pinheiro[15]). Such micromodels have been widely used to study multiphase flows in porous media.[16,17]

Frey et al. used a network (66×121 mm) containing about 15,000 ducts with seven classes of width (from 0.1 to 0.6 mm) distributed log-normally. The distance between two sites of the network was $l \cong 1$ mm. The duct depth was 1 mm. The duct orientations, related to the average direction of the main flow, were 45°. The porosity ε of the micromodel was about 60% and the permeability was about 3×10^{-9} m^2. It should be noted that the micromodel cannot be considered as a Hele–Shaw cell[18] because the depth of the micromodel is not small enough compared to the mean size of the collectors.

Figure 1 shows the layout of the apparatus from which the operating method can be deduced. The suspension was allowed to flow from a constant head vessel. The effluent was collected in another constant head vessel and the overflow was weighted on an electronic balance to determine the flow rate. The total

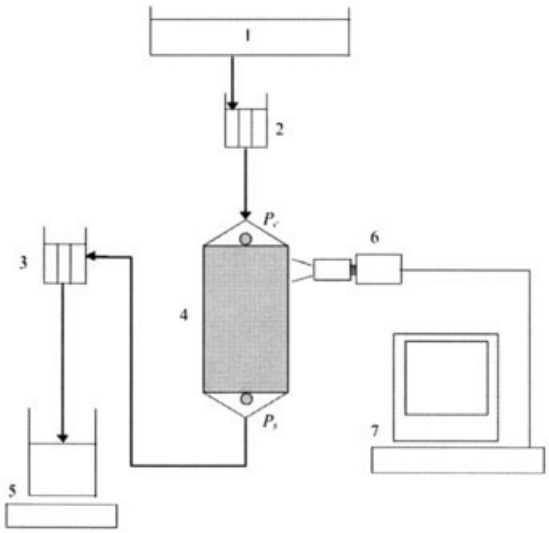

Figure 1. Experimental apparatus.

Legend: (1) Feed tank; (2, 3) constant head vessels; (4) etched micromodel; (5) balance; (6) video camera; (7) computer; P_e, P_s: pressure measurements.

head difference causing the flow was kept constant. The subsequent pressure drop across the micromodel was measured by a differential micromanometer between P_e and P_s. In experiments reported herein, the pressure drop was equal to 420 Pa. When the micromodel was clean, it corresponded to a superficial velocity u_s (averaged in the depth of the micromodel) equal to 10 mm/s.

The suspension was prepared from a dilute solution of KCl (0.01 M) and nonbuoyant Rilsan® particles, which consist of granules with a mean diameter d_p of 0.03 mm (see the scanning electron micrograph on Figure 2). For the entire set of experiments, particle concentration was set at 1 g/L.

A CCD camera was used to visualize particle deposition in the pore systems during each experiment. Images were recorded at prescribed times and posttreated. The domain of interest is a rectangle of 8.5 × 11.3 mm (the first dimension corresponds to the average direction of the main flow), allowing simultaneous observation of about 8 × 11 interconnected pores of the network.

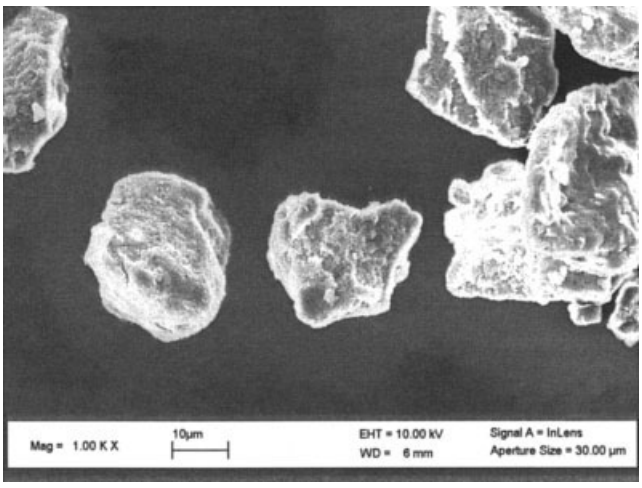

Figure 2. Scanning electron micrograph showing some typical Rilsan® particles.

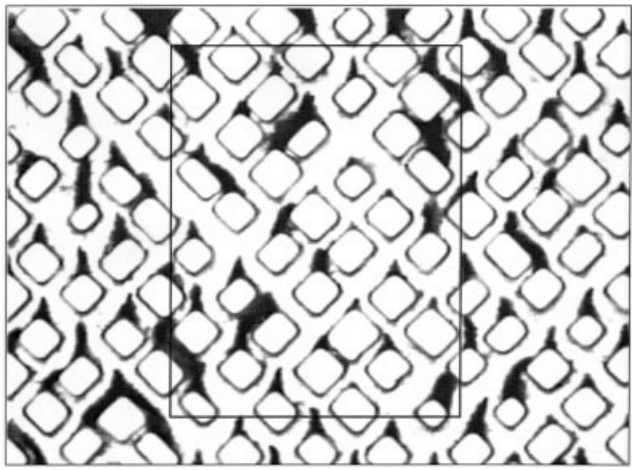

Figure 3. Image of the medium region of the micromodel before clogging occurs.

Let us focus on deposit formation at the beginning of the operation. Deposition generally started close to the upstream region of the solid grains of the porous medium, that is, in the separation region of flow where stagnation points were encountered. A typical image of the porous medium before clogging occurs is presented in Figure 3. This image was recorded in the medium region of the micromodel. At the end of the process, the flow structure inside the porous medium was completely modified and particles accumulated anywhere in the pore space. The complex situations encountered in this latter case are beyond the scope of the present study.

Analysis of the deposition mechanisms

Deposition is a two-step process involving the transport of the suspended particles to the filter and their attachment to the surface of the filter itself.

Let us look at all the forces acting on particles and identify the main transport mechanisms.[1]

Concerning the hydrodynamics, the fluid flow in the experiment was laminar, close to the creeping regime, given that the Reynolds number $\mathrm{Re} = u_s d_c/\nu$ was about 3, where $u_s = 10$ mm/s and d_c, the average channel width, is equal to 0.3 mm in the experiments. The particle Reynolds number $\mathrm{Re}_p \cong u_s d_p/\nu$ was about 0.3, which means that the classical Stokes law is a good approximation of the steady drag force experienced by the particle when it is far from solid boundaries. The Stokes number $N_{\mathrm{St}} = \rho_p d_p^2 u_s/18\rho\nu d_c$ is about 10^{-3}, meaning that the inertial effect (the contribution of the particle acceleration term in Newton's second law) is weak compared with the steady drag force. The forces induced by the liquid inertia (the added mass force, the Tchen force, and the lift force) were also negligible compared to the steady drag force. Indeed, the ratio of the forces arising from liquid inertia to the drag force scales as $d_p^2 u_s/\nu d_c \cong (\rho/\rho_p)\ N_{\mathrm{St}} \cong 10^{-3}$ (this ratio can be also interpreted as a Stokes number calculated for a sphere of fluid of diameter d_p). Finally, we tried to estimate the ratio of the history (or Basset) force to the steady drag force F_H/F_D. Assuming that the suspended particle experienced a step variation

of its velocity of about d_p (u_s/d_c) (the fluid velocity gradient is of the order of u_s/d_c), the forces ratio F_H/F_D scales as $\mathrm{Re}_p^{1/2} \cdot (d_p/d_c)$ after a displacement of the particle of the order of d_p. In the experiments described earlier, the ratio F_H/F_D falls to about 5×10^{-2} over a distance of one particle diameter. Therefore, we can assume that the trajectories of the particles are weakly affected by the history force.

The gravity force did not exist because Rilsan® particles are nonbuoyant. Thus, the gravitational number $N_G = (\rho_p - \rho)d_p^2 g/18\rho\nu u_s$ is null. Brownian motion was negligible compared to convective motion because the Peclet number $\mathrm{Pe} = 6\pi\rho\nu u_s d_p^2/kT$ was about 10^7. The surface forces controls the attachment of particles on the filtering medium but it is negligible compared to the hydrodynamic forces when the particles flow inside the porous medium. Indeed, the London number $N_{\mathrm{LO}} = 4H/9\pi\rho\nu d_p^2 u_s$ (ratio of the London–van der Waals force exerted by the medium on the particle at a separation of the order of d_p to the hydrodynamic force in the Stokes approximation) is about 10^{-8} (the Hamaker constant H is of the order of 10^{-19} J) and the double-layer parameter $N_{DL} = \kappa d_p$ (ratio of the particle diameter to the Debye–Hückel thickness κ^{-1}) is about 10^4.

The interception mechanism can be quantified by the interception number $N_R = d_p/d_c$; thus, $N_R = 0.1$. Because the former mechanisms are negligible, the interception mechanism is the unique transport mechanism in the experiments. Thus, the particles follow the streamlines of the flow and some of them are intercepted by the filter walls under screening conditions.

Finally, we focus on the attachment step and its opposite, that is, the removal step. Considering a particle in contact with the filtering media, three removal mechanisms can occur: sliding, rolling, or lifting. Because the present particles are small and not spherical, sliding is the most probable reentrainment mechanism.[19] The critical drag force F_D^c leading to the removal of a particle satisfies the following force balance

$$F_D^c = f_0(F_{Ad} - F_L) \cong f_0 F_{Ad} \tag{1}$$

where F_{Ad} is the adhesion force; F_L is the lift force, which can be neglected here; and f_0 is the static friction coefficient.

Then, the Mackrle number[20] can be defined as the ratio of the solid friction force, that is, $f_0 F_{Ad}$, to the current drag force suffered by a particle in contact with the filtering media. The drag force experienced by a particle in contact with a plane in a linear shear flow is given by

$$F_D = 3\pi K_D d_p^2 \tau_p / 2 \tag{2}$$

where τ_p is the wall shear stress and K_D is a corrector factor[21] equal to 1.7009.

Assuming Poiseuille flow in the channels of the micromodel, an estimate of the wall shear rate is given by $6u_s/\varepsilon d_c$.

Thus, the Mackrle number can be rewritten as follows

$$\mathrm{Ma} = \frac{f_0 F_{Ad} \varepsilon d_c}{9\pi K_D d_p^2 \rho\nu u_s} \tag{3}$$

Girard[22] studied the adhesion of Rilsan® particles ($d_p = 0.03$ mm) on a glass surface immersed in water using a shear stress flow chamber and measured the critical drag force leading to particle removal, that is, $F_D^c = 1.7 \times 10^{-9} N$.

Thus, the value of the Mackrle number can be estimated under the experimental conditions of Frey's experiments, that is, Ma = 0.7. Because the Mackrle number is of the order of unity, the attachment step cannot be considered as 100% efficient and reentrainment must be taken into account.

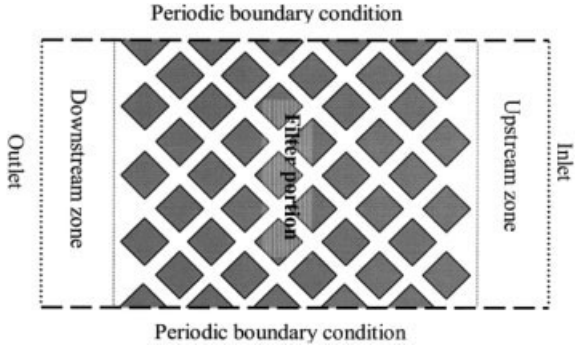

Figure 4. The computational domain.

Modeling

The present model describes the initial phenomena of filtration in a representative elementary volume (REV) of the filter, that is, the transparent micromodel (we assume implicitly that the filter medium is sufficiently homogeneous that we are able to define a REV). The REV is large compared with the pore or grain (that is, the collector) size but small compared to the deep-bed scale. The main advantage of the present approach over the standard microscopic approach is that the coupling effects between the individual collectors are taken into account. In this sense, the present model closely approaches that of Brémond et al.[23] and Tian and Guthrie.[24]

Throughout this investigation, the numerical simulations were performed in two dimensions. Thus, the fluid velocity profile in the channels is underestimated compared to the real one (for a given value of the superficial velocity). However, the streamline pattern deriving from the two-dimensional calculation should be close to the real streamline pattern at least in the median plane of the micromodel. Because most of the particles entering the micromodel move along the median plane (first, because the fluid velocity is the highest in the median plane; second, because the hydrodynamic forces, arising from the velocity gradient in the depth of the micromodel, tend to confine the particles near the median plane), a two-dimensional approach should already provide a relevant description of the particle trajectories. Full three-dimensional calculations are left for a future work.

As can be seen in Figure 4, the computational domain is rectangular and constitutes three parts: the upstream zone, the filter portion, and the downstream zone. The filter portion is defined at the pore scale; the upper frontier of the domain corresponds to the inlet; and the lower frontier to the outlet and periodic boundary conditions are assumed on the lateral sides of the domain.

A typical simulation can be sketched as follows: as a first stage, the flow field is computed in the whole complex void space of the filter using a lattice–Boltzmann method; as a

second stage, the trajectory analysis is derived by applying Newton's second law to suspended particles in the flowing fluid. Each particle is randomly injected upstream and tracked up to its capture site or its filter leaving. A large number of particles ($\sim 10^6$) were investigated to provide meaningful statistical results.

Fluid flow

The fluid is assumed to be Newtonian and the flow incompressible and isothermal. Then, the fluid flow is described by the continuity and Navier–Stokes equations, expressed respectively as

$$\nabla \cdot \vec{j} = 0 \tag{4}$$

$$\frac{\partial \vec{j}}{\partial t} + \frac{(\vec{j} \cdot \nabla)\vec{j}}{\rho} = -\nabla P + \nu \Delta \vec{j} \tag{5}$$

where t denotes the time, $\vec{j}$ is the fluid momentum, P the dynamic pressure, ρ the fluid density (which is constant), ν its kinematic viscosity (which is constant), ∇ the Nabla vector, and Δ the Laplacian operator.

The fluid flow is also supposed to be in a steady state but the nonstationary term is kept in Eq. 5 according to the numerical method used herein.

Equations 4 and 5 are simulated using the lattice–Boltzmann method (LBM) because this method is particularly suitable for investigating fluid flow at low values of the Reynolds number in complex geometry.

The LBM is built as follows: first of all, the d-dimensional space ($d = 2$ in our case) is mapped on a regular lattice. Two types of lattice nodes are distinguished: the first type is attached to the solid porous medium, the second type to the space (in particular the pores of the filter) filled by the fluid. A population of fictitious particles is allocated to each node of the space left to the fluid; the velocity distribution of the population is discrete and constitutes b given velocity vectors. One velocity vector is the null vector and the other velocity vectors are associated with the links between a node and its $(b - 1)$ first and second neighbors. At each time increment, the dynamics is divided into two steps: propagation of the fictitious particles from node to node according to their velocity, then collision between the particles located at the same node. The lattice–Boltzmann model thus has a completely discrete phase space and time. Furthermore, it is formulated to asymptotically recover the Navier–Stokes equations as the large-scale behavior of the LBM (that is, the fictitious particles).

In this study, the version of the LBM first proposed by Qian et al.,[25] with a cubic lattice in two dimensions and nine velocities—D2Q9 in the terminology of Qian et al.—is used. In this version, the collision operator is modeled following the approximation proposed by Bhatnagar, Gross, and Krook[26] (BGK) for the standard Boltzmann equation, that is, it is linearized around the local equilibrium distribution assuming a single relaxation parameter. As usual, the lattice spacing is used as the unit length and the time step as the unit time. Then, the evolution equation for the LBM density can be expressed as

$$N_i(t + 1, \vec{r} + \vec{c}_i) = (1 - \omega) N_i(t, \vec{r}) + \omega N_i^e[\tilde{\rho}(t, \vec{r}), \vec{j}(t, \vec{r})] \tag{6}$$

where $\vec{r}$ and t are the position vector and the time (rendered dimensionless), respectively; N_i is the density of particle i and $\vec{c}_i$ is its velocity; and ω is the relaxation parameter, which lies between 0 and 2 for linear stability. The viscosity of the LBM is all the smaller, given that ω is close to 2. N_i^e is the equilibrium distribution. It is calculated from the total density $\tilde{\rho}(t, \vec{r})$ of particles and the momentum $\vec{j}(t, \vec{r})$ of the fluid at time t and at the node defined by the position vector $\vec{r}$. $\tilde{\rho}(t, \vec{r})$ and $\vec{j}(t, \vec{r})$ are dimensionless quantities. N_i^e is given formally by[27]

$$N_i^e(\tilde{\rho}, \vec{j}) = t_p^*(c_s^2 \tilde{\rho} + \vec{j} \cdot \vec{c}_i) + 3t_p \frac{3(\vec{j} \cdot \vec{c}_i)^2 - \vec{j}^2}{2\rho} \tag{7}$$

The index p is the square modulus of a particle's velocity and is thus equal to 0, 1, or 2. The t_p^* and t_p values are $t_0^* = (3 - 5c_s^2)/3c_s^2$, $t_0 = 4/9$, $t_1^* = 3t_1 = 1/3$, and $t_2^* = 3t_2 = 1/12$. c_s is the intrinsic speed of sound of the LBM and is taken equal to $1/\sqrt{3}$. ρ is the dimensionless density of the fluid, which is constant as the fluid is incompressible and equal to 1. The kinematic viscosity ν of the fluid (in lattice units) is related to the relaxation parameter ω by

$$\nu = \frac{1}{6}\left(\frac{2}{\omega} - 1\right) \tag{8}$$

At each node of the lattice, the pressure P of the fluid and its macroscopic velocity $\vec{u}$ are given, respectively, by (in lattice units)

$$P(t, \vec{r}) = c_s^2 \tilde{\rho}(t, \vec{r}) = c_s^2 \sum_{i=0}^{i=8} N_i(t, \vec{r}) \tag{9}$$

$$\vec{u}(t, \vec{r}) = \vec{j}/\rho = \sum_{i=0}^{i=8} N_i(t, \vec{r}) \vec{c}_i/\rho \tag{10}$$

The lattice must be fine enough to describe the filter medium at the pore scale and to represent precisely the structure of the fluid flow. At the same time, the study of the suspended particles (as opposed to the fictitious particles of the LBM) requires a lattice that describes the filter at the particle scale. A lattice spacing Δx (in real units) that satisfies Eq. 11 meets both requirements and gives reliable results:

$$\Delta x \leq d_p/5 \tag{11}$$

where d_p is the suspended particle mean diameter.

To recover the Navier–Stokes equation as the macroscopic behavior of the LBM, the macroscopic velocity (in lattice units) must be much smaller than the intrinsic speed of sound of the LBM. This involves a constraint on the time step Δt used in the LBM (in real units)

$$\frac{u_{\max}}{\Delta x/\Delta t} \leq \frac{c_s}{10} \qquad \text{that is, } \Delta t \leq \frac{c_s \Delta x}{10 u_{\max}} \tag{12}$$

where $u_{\max}$ is the maximum velocity reached by the fluid in the domain (in real units).

A flat and constant momentum profile is fixed at the inlet. Thus, the following relation must hold at each boundary node constituting the upper frontier of the domain

$$\vec{j}(t, \vec{r}) = \vec{j}_0 \tag{13}$$

Note that $\vec{j}_0$ is fixed to $\vec{j}_0 = \rho \vec{u}_s$, where $\vec{u}_s$ is the superficial velocity of the fluid in the porous medium. Then, the LBM densities "entering the domain" at each time increment at the inlet are given by

$$N_i(t + 1, \vec{r}) = N_{i'}(t, \vec{r} + \vec{c}_i) + 2t_p^*(\vec{j}_0 \cdot \vec{c}_i) \tag{14}$$

where $N_{i'}(t, \vec{r} + \vec{c}_i)$ is the LBM density coming from inside in the direction i' opposite to the direction i.

A vanishing momentum gradient is assumed at the outlet. Then, the LBM densities "entering the domain" at each time increment at the outlet are given by

$$N_i(t + 1, \vec{r}) = N_i(t + 1, \vec{r} - \vec{c}_1) \tag{15}$$

where the direction 1 of the lattice (and its corresponding velocity $\vec{c}_1$) is taken parallel to the average direction of the main flow.

A no-slip condition is assumed on the solid surfaces, which constitute the filter. This condition is modeled by the so-called bounce-back rule, in which a particle incident on the boundary reverses its direction. In this way, the fictitious particles are kept out of the obstacles and the null velocity condition is satisfied at the solid surface. The solid surface is located halfway between the "fluid node" and the "solid node" forming the obstacle.

Finally, as mentioned earlier, periodic boundary conditions are assumed on the "lateral sides" of the domain.

Suspended particles

The suspended particles are assumed to be rigid and nondeformable. Their concentration is low enough that the interactions between the suspended particles in the liquid are negligible. Then, the suspended particles move independently from each other. Their trajectories are obtained from Newton's second law. The corresponding equations are numerically solved using a Eulerian scheme.

The Newton second law can be written for a non-Brownian suspended particle as follows

$$\frac{\pi}{6} \rho_p d_p^3 \frac{d\vec{u}_p}{dt} = \frac{\pi}{6} \rho_p d_p^3 \vec{g} + \vec{F}_f + \vec{F}_s \tag{16}$$

where ρ_p is the density of the particle, $\vec{u}_p$ is its velocity, and d_p is its diameter. The first term of the right-hand side of Eq. 16 is the gravitational force; $\vec{F}_f$ is the resultant of the forces exerted by the fluid on the surface of the particle; and $\vec{F}_s$ is the surface interactive force between the particle and the filtering medium, which is specifically the London–van der Waals force and the double-layer force for hydrosols.

As seen previously, the particle trajectory is not affected by the surface interactive force until its contact with the filtering medium.

Concerning the force $\vec{F}_f$ exerted by the fluid, there are two general approaches to model it. The first method is based on the solution of the Navier–Stokes equation for the fluid phase because it is coupled to the movement of the suspended particles. This method has been applied in the lattice–Boltzmann framework to suspensions of spherical and ellipsoidal particles.[28-30] Then, $\vec{F}_f$ is calculated from the momentum balance between the suspended particles and the lattice–Boltzmann particles impinging upon them. This method is very general, in that all the hydrodynamical effects are intrinsically taken into account, although it remains computationally intensive even in the LBM framework. Furthermore, such an accurate method is adapted to well-defined particles (spheres or ellipsoids) but it is perhaps too sophisticated for the irregular particles commonly handled in deep filtration.

The second method that has been chosen in the present study consists in breaking down the force exerted by the fluid into fundamental contributions and expressing them analytically in terms of unperturbed flow properties at the location of the suspended particle. Six fundamental contributions are usually identified in $\vec{F}_f$. These contributions are assumed to be simply additive:

$$\vec{F}_f = \vec{F}_A + \vec{F}_D + \vec{F}_H + \vec{F}_M + \vec{F}_{\text{Tchen}} + \vec{F}_L \tag{17}$$

where $\vec{F}_A$ denotes the Archimedes force, $\vec{F}_D$ is the steady drag, $\vec{F}_H$ represents the history (or Basset) force, $\vec{F}_M$ is the added-mass force, $\vec{F}_{\text{Tchen}}$ is the Tchen force, and $\vec{F}_L$ is the lift force.

As in Frey's experiments, the particles are nonbuoyant and particle inertia and flow inertia are negligible; Newton's second law for a particle, which is not in contact with the filtering medium, reduces to

$$\vec{F}_D = 3\pi\rho\nu d_p(\vec{u} - \vec{u}_p) = \vec{0} \tag{18}$$

where the steady drag force $\vec{F}_D$ imparted by the fluid has been modeled by the Stokes formula. Because the particle Reynolds number is small, the Stokes formula is a good approximation of the steady drag when the particle is far from solid boundaries. If the particle is close to a solid boundary, the drag force that it experienced deviates from the Stokes expression as a consequence of the lubrication effect. This phenomenon can be dominating and thus prevent the particle from being captured when the particle surface and the filter surface are smooth. However, for irregularly shaped particles or rough filter walls, the lubrication effect (that is, retardation) on particle transport and capture is assumed to be weak and is neglected. Indeed, it can be asserted that particle singularities (such as edge, vertex, or protuberance) or filter surface asperities will break the lubrication film before lubrication forces strongly affect the particle trajectory.

Thus, the governing equations for particle trajectory are

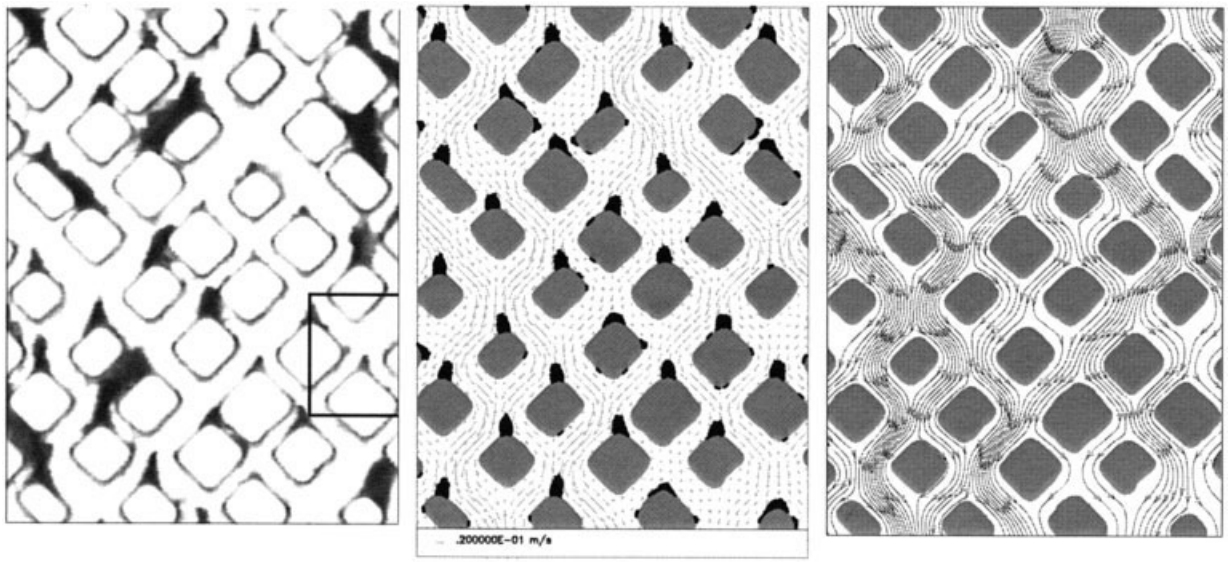

Figure 5. Comparison between the experiments and the numerical results.

Left: experimental deposits. Center: fluid velocity field (in gray) and initial capture probability density (in black). Right: streamline pattern.

$$\vec{u}_p = \vec{u}(\vec{r}_p) \tag{19}$$

$$\frac{d\vec{r}_p}{dt} = \vec{u}_p \tag{20}$$

Equations 19 and 20 are numerically solved using an explicit Eulerian scheme:

$$\vec{u}_p(t_p + \Delta t_p) = \vec{u}[\vec{r}_p(t_p)] \tag{21}$$

$$\vec{r}_p(t_p + \Delta t_p) = \vec{r}_p(t_p) + \vec{u}_p(t_p)\Delta t_p \tag{22}$$

It should be noted that $\vec{r}_p$ and $\vec{u}_p$, the position vector and the velocity vector of a suspended particle, respectively, vary along a continuum. Because the LBM provides a discrete field of the fluid velocity, the velocity of the fluid $\vec{u}(\vec{r}_p)$ at the location of the suspended particle $\vec{r}_p$ is calculated using linear interpolations between the four closest nodes of the lattice.

Each suspended particle is pseudorandomly introduced upstream and its velocity is initially fixed to $\vec{u}_p(0) = \vec{u}_s$, where $\vec{u}_s$ is the superficial velocity of the fluid.

Each particle is essentially following a fluid streamline until both conditions are simultaneously fulfilled:

- The distance from the center of the particle to the wall of the filter, denoted R_p, is equal to or lower than the radius of the particle, that is, $R_p \leq d_p/2$.
- The drag force experienced by the particle in contact with the filtering medium, $F_D = 3\pi K_D d_p^2 \tau_p/2$, is smaller than the solid friction force $f_0 F_{Ad}$.

Then, the particle is definitively captured by the filtering media.

Validation

As a first stage, the above numerical model is used to derive the streamline pattern in the micromodel of Frey et al. Then, the initial capture probability density provided by the numerical simulation is compared to the experimental deposits obtained in the initial stage of filtration. Finally, the dependency of the initial filter coefficient on the pitch l of the micromodel is investigated.

Streamline analysis

A careful analysis of the streamline pattern should improve our understanding of particle deposition at the beginning of the filtration. For this purpose, the present model is used to simulate the fluid flow in a part of the transparent micromodel; the investigated domain is the porous medium presented in Figure 3: a rectangle of 8.5 × 11.3 mm, located in the medium region of the micromodel. The porous medium has been weakly modified laterally so that the left edge "fit" the right one (trying to conserve the same porosity as the full micromodel). This ensures "smooth" periodic boundary conditions laterally. The corresponding computational domain consists of 1925 × 1959 nodes: the filter portion consists of 1525 × 1959 nodes and the upstream and downstream zones constitutes each of them 200 × 1959 nodes. The lattice spacing Δx is equal to 5 μm.

Figure 5 (right) displays the streamline pattern in a part of the computational domain. The streamlines have been obtained from the calculated velocity field using the commercial software Tecplot®.

Streamline analysis showed different possibilities of particle deposition. Let us focus on the pore displayed in Figure 6. The flow is divided into three regions. The first flow region (the light gray domain on the left in Figure 6) concerns the fluid coming from the whole top left channel that feeds the left part of the bottom left channel. The third flow region (the light gray domain on the right) concerns the right part of the fluid coming from the top right channel that feeds the whole bottom right channel. The intermediate region (in white in Figure 6), that is, the second flow region, concerns the left part of the fluid coming from the top right channel that feeds the right part of the bottom left channel. Because the downstream grain is

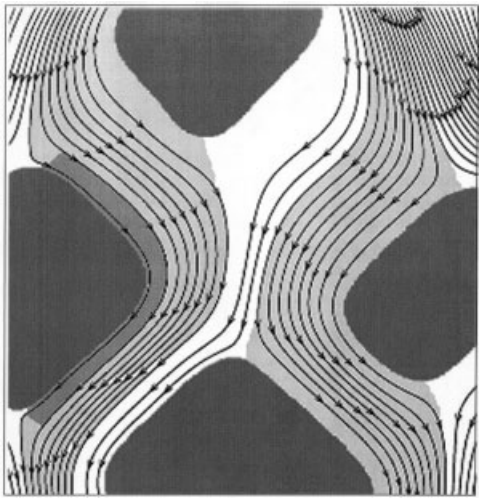

Figure 6. Streamline pattern in a pore.

completely wetted by the fluid coming from the top right channel, there is a dividing streamline, which comes from the top right channel and finishes at the tip of the downstream grain. We may assume that some particles accumulate at this separation point along the dividing line. The deposits occurred on each grain and were able to invade the pore until they reached either the opposite or the neighboring grain, then clogged the gap separating the two grains. This type of deposit will be named "pore invasion deposit." [14] Even though these deposits initially pointed upstream of main flow, some became progressively curved because of the modification of the local flow field, in particular to clog the throats of shorter width.

In some cases, it may be noticed that the distance between the streamlines in the exit channel (the bottom left channel in Figure 6) is less than that in the inlet channel (the top left channel in Figure 6). In these cases, for a particle at a distance R_p from the wall in the inlet channel, the corresponding distance at the channel exit will be less than R_p (the domain of interest is displayed in medium gray in Figure 6). Thus, we may assume that such particles will deposit between the inlet channel and the exit channel. Actually, these deposits appear at the inlet channel wall close to the corner of the upstream grain. This kind of deposit often occurs when the throat size ratio is small. Furthermore, experimental observations provide evidence that these deposits grow downstream until they eventually invade the exit channel. This type of deposit is called "throat invasion deposit." [14] Compared to pore invasion deposit, throat invasion deposit is less frequent.

Deposit shape and location

Some 1,000,000 particles have been injected upstream to obtain the map of the initial capture probability density. To qualitatively compare numerical and experimental results, we represent the initial capture probability density around each grain as a "pseudodeposit" (see Figure 7): let us call M_w the impact point on the grain. The corresponding external point of the "pseudodeposit" M_e is such that: $\overrightarrow{M_wM_e} = C\Pi\vec{n}$, where $\vec{n}$ is the normal to the obstacle at the impact point M_w, Π is the capture probability density at the impact point (Π is proportional to the ratio of the number of particles that impact in the vicinity of M_w to the total number of particles injected upstream), and C is a proportionality factor that is the same for each impact point and is adjusted to optimize the legibility of the map.

Figure 5 (left, center) shows that the pore invasion deposit shape and location are highly correlated to the initial capture probability density. The present model forecasts particle deposition on the top of most grains. This prediction is confirmed by the experimental results. The deposits tend to invade the pore space.

Concerning the throat invasion deposits, the location is also well correlated to the initial capture probability density. The occurrence of throat invasion deposits is in concordance with the experimental findings. This agreement confirms that the lubrication effect can be reasonably neglected when the particles are irregularly shaped. It should be noted that a stronger lubrication effect would affect the capture of the particles by the channel walls and decrease the occurrence of throat invasion deposits, but would not influence the formation of pore invasion deposits because they occur at the stagnation points of the micromodel.

The shape and the relative size of the throat invasion deposits are weakly correlated to the initial capture probability density. Indeed, the mechanism of particle deposition changes between the initiation of the throat invasion deposit and its subsequent growth[14]: at the beginning, the first particles that impact the channel wall create an obstacle that generates two stagnation points at the front and at the back where other particles can progressively accumulate with a kind of snowball effect. Therefore the initial capture probability density is not able to predict the corresponding deposit occurring from the modification of the local flow because of the appearance of new obstacles.

Initial filter coefficient

In addition to the above-mentioned microscopic results, the present model provides macroscopic data that could be entered in a macroscopic model of deep filtration, such as the permeability or the initial filter coefficient. For example, the initial filter coefficient relative to operating conditions used by Frey et al. has been calculated and a sensitivity study has been set up. Because Frey et al. did not precisely measure the influent and effluent particle concentrations, the numerical results have

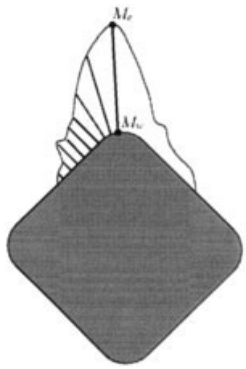

Figure 7. Representation of the initial capture probability density around a grain as a "pseudodeposit."

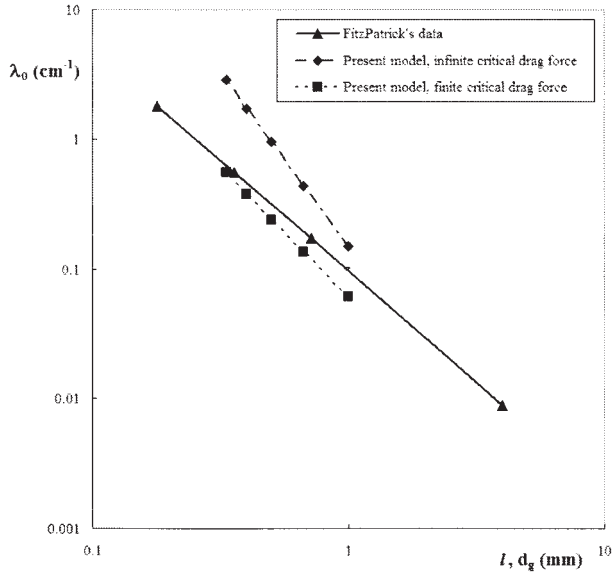

Figure 8. Dependency of initial filter coefficient on the pitch *l* (micromodel) or on the filter grain diameter d_g (glass-spheres filter).

been compared to data obtained by FitzPatrick and reported by Tien.[1] FitzPatrick studied the filtration of monodispersed latex particles on unisized glass-spheres filters and determined the particle concentration at the inlet and outlet with a Coulter counter. The data set that has been selected was obtained under conditions very close to those of Frey et al.: the superficial velocity is equal to 3 mm/s; the particle diameter is equal to 0.021 mm; and the glass-sphere diameter is equal to 0.18, 0.36, 0.72, or 4 mm.

According to FitzPatrick's results, which show the effect of the filter grain size, we studied the effect of the pitch l of the network of ducts on the initial filter coefficient. Thus, we performed numerical simulations with homothetic micromodels, while keeping all the other parameters constant. The homothetic ratio is equal to 1, 2/3, 1/2, 2/5, or 1/3.

The initial filter coefficient λ_0 is calculated according to the following expression

$$\lambda_0 = -\ln(1 - E_0)/L \tag{23}$$

The initial filtration efficiency E_0 is calculated over a depth $L = 6$ mm, when the total depth of the filter portion is 8.5 mm. In this way, we avoid a potential "edge effect." Then, E_0 is given by

$$E_0 = (n_a - n_b)/n_a \tag{24}$$

where n_a (respectively, n_b) is the number of particles that are still free 1.25 mm after (before) the inlet (outlet) of the filter portion.

The numerical simulations have been performed for infinite and finite critical drag force. In the latter case, the critical drag force is fixed to Girard's value,[22] that is, $F_D^c = 1.7 \times 10^{-9}N$.

The relationships between λ_0 and the pitch l or the grain diameter d_g are shown in Figure 8. For the three curves, we observe that λ_0 becomes smaller for larger values of the pitch l or for larger values of the grain diameter d_g. However, the dependency on l or d_g is stronger when the adhesion is 100% efficient (infinite critical drag force). Thus, the dependency of λ_0 on l is given by

$$\lambda_0 \sim l^{-2.67} \tag{25}$$

Using appropriate dimensionless numbers, $\lambda_0 l$ and N_R, this relation is equivalent to

$$\lambda_0 l \sim N_R^{1.67} \tag{26}$$

The power of 1.67 is intermediate between the first power given by the capillaric model[31] and the second power given by the spherical model.[1]

On the other hand, FitzPatrick's experimental data and the numerical results obtained for $F_D^c = 1.7 \times 10^{-9}N$ have a weaker dependency on l or d_g, respectively

$$\lambda_0 \sim d_g^{-1.72} \tag{27}$$

$$\lambda_0 \sim l^{-2.01} \tag{28}$$

Indeed, as the filter grain diameter decreases, the wall shear rate increases (the superficial velocity being fixed), then the Mackrle number—which quantifies the adhesion efficiency—decreases and the increase of the initial filter coefficient is slower than expected. Thus, considering the experiments conducted by Frey et al., the following scaling law of the dimensionless initial filter coefficient can be proposed

$$\lambda_0 l \sim N_R^{1.67}\mathrm{Ma}^{0.66} \tag{29}$$

Three main reasons can be set forth to explain the gap between the exponents of scaling laws 27 and 28: (1) it can be attributed to the "microscopic" geometry itself, which varies from FitzPatrick's filter to that of Frey et al., and can lead to somewhat different interception contributions; (2) the adhesion force is assumed to be constant even if it may vary with the curvature radius of the obstacle and therefore decreases as the micromodel pitch decreases; and (3) the drag force experienced by a particle in a channel is substantially enhanced when the ratio of the particle diameter to the channel width becomes >0.1. This effect is not taken into account by the present model.

Conclusions

A lattice–Boltzmann model of depth filtration has been developed. For the moment, the present model is based on the following assumptions: the filter is a two-dimensional porous medium, only the initial stage of filtration is described, the fluid-particle suspensions are hydrosols, the suspended particles are assumed to be non-Brownian and nonbuoyant, the force exerted by the fluid reduces to Stokes steady drag, and the lubrication effects are neglected. However, none of these assumptions is definitive: the extension to three-dimensional porous media, as well as the extension to the ageing stage, and

the integration of the lubrication effect (by using the hydrodynamic correction functions reported in the literature) are already in hand.

The model was applied to a model experiment of deep-bed filtration in which the porous medium is a transparent etched network of interconnected channels, allowing the deposit visualization at pore scale. The initial capture probability density provided by the numerical simulation was compared to experimental observations obtained in the initial stage of filtration. The present model gives a correct description of the location of the deposits observed experimentally and, to a certain extent, of their shape. This indicates that the effect of lubrication on deposition is weak when the particles are irregularly shaped or when the filter walls are sufficiently rough (and it will be even weaker if particles are buoyant as well). The precise dependency of the lubrication effect on the particle shape and on the filter roughness is left for future work.

Finally, the influence of the filter grain diameter on the filter coefficient has been investigated numerically: the scaling behavior of the filter coefficient is in good agreement with experimental data reported in the literature.

Thus, the present model can be an appealing tool for predicting the performance of filters and for optimizing the filtration process (such as the value of the operating process parameters, the choice of the filters, and the design of new filter geometries).

Literature Cited

1. Tien C. *Granular Filtration of Aerosols and Hydrosol*. 1st Edition. Boston, MA: Butterworths/Reed Publishing; 1989.
2. Herzig JP, Leclerc DM, Le Goff P. Flow of suspensions through porous media—Application to deep bed filtration. *Ind Eng Chem.* 1970;62:8-35.
3. Iwasaki T. Some notes on sand filtration. *J Am Water Works Assoc.* 1937;29:1591-1602.
4. Johansen ST, Anderson NM. A mathematical model for large scale filtration. In: Gaskell DR, ed. Proc of the TMS Annual Meeting—EPD Congress '90, Feb. 19–22, Anaheim, CA, The Minerals, Metals & Materials Society; 1990:441-451.
5. Payatakes AC, Tien C, Turian RM. A new model for granular porous media, I: Model formulation. *AIChE J.* 1973;19:58-76.
6. Acosta GFA, Castillejos EAH, Almanza RJM, Flores VA. Analysis of liquid flow through ceramic porous media used for molten metal filtration. *Met Trans B.* 1995;26B:159-171.
7. Fan LT, Nassar R, Hwang SH, Chou ST. Analysis of deep bed filtration data: Modeling as a birth–death process. *AIChE J.* 1985;31: 1781-1790.
8. Leitzelement M, Maj P, Doods JA, Greffe JL. Deep bed filtration in a network of random tubes. In: Gregory J, ed. *Solid–Liquid Separation*. Chichester, UK: Ellis Horwood; 1984:273-296.
9. Rege SD, Fogler H. S. Network model for straining dominated particle entrapment in porous media. *Chem Eng Sci.* 1987;42:1553-1564.
10. Rege SD, Fogler HS. A network model for deep bed filtration of solid particles and emulsion drops. *AIChE J.* 1988;34:1761-1771.
11. Ghidaglia C, de Arcangelis L, Hinch J, Guazzelli E. Hydrodynamic interactions in deep bed filtration. *Phys Fluids.* 1996;8:6-14.
12. Ghidaglia C, de Arcangelis L, Hinch J, Guazzelli E. Transition in particle capture in deep bed filtration. *Phys Rev E.* 1996;53:R3028-R3031.
13. Rothman DH, Zaleski S. *Lattice-Gas Cellular Automata*. 1st Edition. Cambridge, UK: Cambridge Univ. Press; 1997.
14. Frey JM, Schmitz P, Dufreche J, Gohr Pinheiro I. Particle deposition in porous media: Analysis of hydrodynamics and weak inertial effects. *Transport Porous Media* 1999;37:25-54.
15. Gohr Pinheiro I. *Transport et dépôt de particules en milieu poreux: de l'échelle de pore à l'échelle macroscopique*. PhD Thesis. Toulouse, France: Institut National Polytechnique de Toulouse; 1996.
16. Lenormand R, Zarcone C, Sarr A. Mechanisms of the displacement of one fluid by another in a network of capillary ducts. *J Fluid Mech.* 1983;135:337-353.
17. Lenormand R, Touboul E, Zarcone C. Numerical models and experiments on immiscible displacements in porous media. *J Fluid Mech.* 1988;189:165-187.
18. Guyon E, Hulin JP, Petit L. *Hydrodynamique Physique*. 1st Edition. Paris, France: InterEditions/Editions du CNRS; 1991.
19. Cardot J, Blond N, Schmitz P. Adhesion and removal of particles from surfaces under humidity controlled air stream. *J Adhes.* 2001;75:351-368.
20. Zimon AD. *Adhesion of Dust and Powder*. 1st Edition. New York, NY: Plenum Press; 1969.
21. O'Neill ME. A sphere in contact with a plane wall in a slow linear shear flow. *Chem Eng Sci.* 1968;23:1293-1298.
22. Girard P. *Caractérisation de l'adhésion de particules sur une surface plane*. DEA Dissertation. Toulouse, France: Institut National Polytechnique de Toulouse; 1994.
23. Brémond R, Jeulin D, Abouaf M, His C. Simulation de la filtration de la fonte. *Rev Métall-CIT/Science Gén Matér.* 1995;5:594-606.
24. Tian C, Guthrie RIL. Direct simulation of initial filtration phenomena within highly porous media. *Met Trans B.* 1995;26B:537-546.
25. Qian YH, d'Humières D, Lallemand P. Lattice BGK models for Navier–Stokes equations. *Europhys Lett.* 1992;17:479-484.
26. Bhatnagar PL, Gross EP, Krook M, A model for collision processes in gases. I. Small amplitude processes in charged and neutral one-component systems. *Phys Rev.* 1954;94:511-525.
27. Ginzburg I, d'Humières D. Multi-reflection boundary conditions for lattice Boltzmann models. *Phys Rev E.* 2003;68:066614-1-30.
28. Ladd A. Numerical simulations of particulate suspensions via a discretized Boltzmann equation. Part 1. Theoretical foundation. *J Fluid Mech.* 1994;271:285-309.
29. Ladd A. Numerical simulations of particulate suspensions via a discretized Boltzmann equation. Part 2. Numerical results. *J Fluid Mech.* 1994;271:311-339.
30. Aidun C, Lu Y, Ding J. Direct analysis of particulate suspensions with inertia using the discrete Boltzmann equation. *J Fluid Mech.* 1998; 373:287-311.
31. Payatakes AC, Rajagopalan R, Tien C. Application of porous media models to the study of deep bed filtration. *Can J Chem Eng.* 1974;52: 722-731.

Manuscript received Jan. 7, 2004, and revision received May 16, 2005.